The quantification of navigation independent neuronal phase precession

By

Connor Stephen Braun

Under the supervision of

Dr. Wilten Nicola

A THESIS SUBMITTED IN PARTIAL FULFILMENT OF THE REQUIREMENTS OF THE BACHELOR OF SCIENCE HONOURS IN NEUROSCIENCE PROGRAM

BSc Neuroscience Program
Faculty of Science
University of Calgary

January 2 2022

Abstract

Phase precession as a phenomenon has been strictly associated with place cells and spatial behaviors since it's discovery nearly thirty years ago. Despite this, phase precession has long been known to bestow place cells with phase coding properties with respect to a local theta oscillation. At it's outset, the project was aimed at finding phase precession outside of the context of spatial behaviors and hopefully establish new contexts in which phase coding can be experimentally investigated. Problematically, there does not exist a method for quantifying phase precession in data without first knowing the behavior to which the neuron is tuned. Hence, before phase precession can be studied independent of the remarkably specific behavioral tuning of place cells, some behavior-independent quantification needs to be developed. Currently, we have designed an algorithm to quantify all types of neuron-phase relationships which is agnostic to organism behavior. A model has been developed to capture key biological characteristics of place cells, and to controllably exhibit various phase-relationships with an artificial theta oscillation using a dual oscillator interference model. Preliminary results suggest that our algorithm reliably quantifies neuron-phase relationships, but with some evidence of erroneous results under niche conditions. Furthermore, the observed results are invariant under adjustment of model spike frequency adaptation parameters. Next, we will more rigorously assess algorithm error before making final adjustments to it. The algorithm will then be ready for use in quantifying place cell phase precession in animals undergoing spatial behavior, with the results compared to convential phase precession quantification methods in the same data and algorithmic quantification of neuron-phase relationships in non spatial data.

Introduction

The hippocampal formation is known to host computations involved in both navigation and memory consolidation (Scoville & Milner 1957, O'Keefe 1976) the latter of which is thought to be principally supported by place cells, which exhibit highly specific tuning to organism position in space (O'Keefe 1976, Muller et al. 1994). We call such an environmental position to which a place cell is tuned the cell's place field. While it is not known what upstream influences mediate this tuning (sensed environmental features versus some abstract representation of position) the properties of place cell tuning may offer tremendous experimental opportunity to glean insight on neural coding at large. It is generally prudent to exercise restraint when considering the significance of single-unit coding in behavior and cognition. However, in addition to the prominent spatial-coding properties of place cells, it has been demonstrated that even small populations of place cells under optogenetic manipulation can influence motoric behavior in rats in a manner predicted by their behavioral tuning during a navigational task (Robinson et al. 2020). Since these neurons are not directly modulating motor behaviors, they are instead thought to interface with memory to influence the decisions of an animal based on past experience. Understanding how single unit coding translates to network-level function remains a considerable challenge, however the observation that even small hippocampal subnetworks (15-20 neurons, in the aforementioned study) hold such sway over high level function bestows great significance to the dynamics of place cells as mechanisms of information encoding.

For the last thirty years, hippocampal place cells have been observed to form robust phase relationships with theta-range (8-12 Hz) local field potential oscillations (O'Keefe & Recce 1993). These oscillations permeate the hippocampal cortex, varying in phase and amplitude as a function of the depth of recording (Bullock et al. 1990) and modulate activity of all types of neurons in the hippocampal milieu (Bland et al. 1975, Fox et al. 1986). Specifically, active place cells exhibit a phenomenon known as phase precession with respect to local theta oscillations as an organism traverses a corresponding place

field. That is, subsequent place cell bursts occur progressively earlier on the concurrent theta cycle. In addition, place cells exhibit a property known as phase coherence, which is their propensity to begin bursting shortly after maxima of the local theta oscillation – corresponding to the moments of lowest local inhibitory interneuron activity (Skaggs et al. 1996). Hence, place cell coding is rich with temporal characteristics imparted to it by the direct and distributed influence of theta oscillations, motivating the hypothesis that it is not the spike train characteristics of a single neuron, but the coordination of place cell activity which encodes temporospatial information.

One such hypothesis which precipitates as a natural result of phase coherence and precession was originally argued by Skaggs et al. (1996). Activity of place cells with overlapping place fields reflects the sequence in which their place fields were traversed. Moreover, their activity is repeated on individual periods (cycles) of theta on a compressed timescale which is relevant to mechanisms of spike timing dependent plasticity (Levy & Steward 1983). This has long painted phase precession as a means of bestowing sequence structure to memories associated with navigation – namely the order in which a sequence of overlapping place fields were traversed.

Memory temporal structure is not unique to navigation, however. It is eminently clear that temporal order is a feature of most if not all long term episodic memory. Could phase precession then be a more general neurocomputational phenomenon, coordinating the activity of hippocampal cells when their behavioral tuning is unclear? Some very limited evidence exists in support of hippocampal phase precession during REM phase sleep (Harris et al. 2002) but otherwise phase precession has to date been considered a purely navigational phenomenon. The problem is that conventional methods of experimentally quantifying phase precession rely on *a priori* knowledge of neural tuning so that spike timing with respect to a concurrent local theta oscillation can be fit by some function of behavior (O'Keefe & Recce 1993, Schmidt et al. 2009). This curtails our ability to seek phase precession beyond the scope of place cells and navigation since neural tuning needs not have any obvious external correlate, generally speaking. Hence, the present work is focused on first developing a first order metric quantifying phase precession, then using our novel algorithm to seek phase precession dynamics beyond the scope of navigational behavior. This work stands to potentially liberate phase precession as a purely navigational phenomenon, and offer a tool to aid future investigation.

Currently, the algorithm takes an oscillating local field potential and the spike times from a neuron of interest and returns a first order metric indicating the phase relationship between the two inputs. To maximize it's extensibility beyond place cells and navigation, the algorithm is agnostic to organism behavior and is capable of quantifying not just phase precession, but phase locking – where the interburst interval is equivalent to the period of theta – and phase recession where bursts occur progressively later on each subsequent cycle of theta. Therefore, to characterize the biologically-relevant conditions under which our algorithm is type I or type II erroneous, we require a model which consists of an artificial theta oscillation and a spiking neuron which can controllably exhibit phase precession, locking and recession. We call the known phase relationship the ground truth, and expect the return value of our algorithm to reflect it. By it's construction, we intend for negative, approximately zero and positive real numbers to indicate phase recession, locking and precession respectively. The algorithm will be covered in depth in methods.

We next consider the mechanism by which we'll control the model phase dynamics. Several biological mechanisms have been posited to underly hippocampal theta phase precession (Burgess & O'Keefe 2011) but among the biologically compelling models is that of the dual oscillator hypothesis (Lengyel et

al. 2003, O'Keefe & Recce 1993). For modeling and expository purposes, consider the idealized case where two sinusoids are integrated by a single neuron. Then, the equation describing the superposition of these two oscillators (assuming they both have equal amplitude) is given by

$$Asin(\omega_1 t) + Asin(\omega_2 t) = 2Acos\left(\frac{\omega_1 - \omega_2}{2}t\right) sin\left(\frac{\omega_1 + \omega_2}{2}t\right) \tag{1}$$

Where A is the sinusoid amplitude, $\omega_i = 2\pi f_i t$ is the angular frequency of the i^{th} sinusoid, and t is time. The cosine factor in this formula defines the envelope of the interference pattern and has angular frequency $\frac{\omega_i - \omega_2}{2} < \omega_1$, while the sine factor defines the carrier of the interference pattern and has angular frequency $\frac{\omega_1 + \omega_2}{2}$. Taking this to be the forcing function of a neuron model, the result is a maximum spike probability proximal to envelope maxima with intraenvelope spike timing controlled by the carrier wave maxima. Then, taking $Asin(\omega_1 t)$ to represent the theta rhythm and fixing ω_1 to some frequency in the theta band, we have a simple mechanism for forcing various theta phase relationships on a receiving neuron. Within an individual envelope, we can consider neuronal spiking/bursting frequency (depending on intrinsic dynamics) to be approximated by the carrier frequency $\omega_3 = \frac{\omega_1 + \omega_2}{2}$ such that

$$\omega_3 < \omega_1, \quad \text{when } \omega_2 < \omega_1 \text{ (recession)} \tag{2}$$

$$\omega_3 = \omega_1, \quad \text{when } \omega_2 = \omega_1 \text{ (locking)} \tag{3}$$

$$\omega_3 > \omega_1, \quad \text{when } \omega_2 > \omega_1 \text{ (precession).} \tag{4}$$

The dual oscillator model is certainly convenient for modeling purposes, with simple parametric conditions determining model ground truth. However, it should be noted that despite it's biological plausibility (Lengyel et al. 2003) the identity of interference oscillation represented by $Asin(\omega_2 t)$ is not known. Since cornu ammonis 3 (CA3) to cornu ammonis 1 (CA1) recurrent projections via the Schaffer collaterals contribute meaningfully to theta oscillation characteristics (Bragin et al. 1995), with CA3 itself being an intrahippocampal oscillator, it has been speculated that CA3 could act as a second interferring oscillatory influence (Buzsaki 2002). Regardless, the biological reality is unimportant for the purposes of developing a useful algorithm and exploring navigation-independent phase precession.

Methods

All programming was done using Python 3.9 and will be available at a public GitHub repository once the project is finalized. As an overview, the experiment began by first developing a 'base' neuron model and a novel algorithm for quantifying neuron-theta phase relationships. Next, the proposed algorithm was tested. The details of the base model, proposed algorithm and testing methodology will be described in turn.

Hippocampal place cells prominently exhibit bursting with spike frequency adaptation (Ranck 1973, Royer et al. 2012) so we construct a model which captures this behavior. Since the algorithm takes spike times as input, we select a voltage model which is computationally inexpensive and generates well-defined spike times without the need to manually locate extrema. For these reasons, a linear leaky integrate-and-fire neuron model was chosen, with a suprathreshold adaptation current and an Ornstein-Uhlenbeck process (Uhlenbeck & Ornstein 1930) to contribute a stochastic current and heighten the excitability of the model. The complete model is defined by the following system of nonlinear differential equations, described piecemeal.

$$\tau_m \frac{dV}{dt} = -(V - V_r) - W + \xi + I(t) \tag{5}$$

Here we introduce the first two state variables V and t for the membrane potential and time respectively. The function $I(t)$ will be some dual oscillator input of varying amplitude and frequency parameters. The constants here are τ_m and V_r for the membrane time constant and resting potential respectively. The adaptation current W, the next state variable, is governed by the differential equation

$$\tau_W \frac{dW}{dt} = -W_d W + W_r \sum_{t^{(f)}} \delta_{t,t^{(f)}} \tag{6}$$

Where τ_W is the adaptation time constant, W_d and W_r are decay and response constants and $\delta_{i,j}$ is Kronecker delta. Spike times are given by $t^{(f)}$ such that at the moment of a spike the adaptation current increments by W_r, but decrements by W_d regardless of neuron state. For this reason, the model is called suprathreshold adapting. Finally, we have the stochastic influence ξ given by Ornstein-Uhlenbeck process:

$$d\xi = \tau_\xi(\mu - \xi)dt + \sigma\sqrt{dt\tau_\xi}U(\mu,t) \tag{7}$$

Where τ_ξ is the Ornstein-Uhlenbeck time constant, σ is the standard deviation of discrete Weiner process $\sqrt{dt\tau_\xi}U(\mu,t)$, with $U(\mu,t)$ being a number sampled from normal distribution with variance 1 and mean μ at time t. To integrate the system numerically, we use the Euler method with timestep 0.01 milliseconds which generates membrane potential timeseries. Spike times are determined during integration as each moment where membrane potential exceeded threshold V_T. Base model parameters were selected such that the model would exhibit bursts of 1-4 spikes when forced with a pure sinusoid of sufficient amplitude with frequency over the range 6-12 Hz while maintaining the bound $|V| \leq 120$. A summary of base parameters is listed in table 1 and were, in part, informed by previous work quantifying hippocampal pyramidal parameters (Gao et al. 1999, Mason 1993).

The novel precession quanficiation algorithm developed will be referred to as the return map quanficiation (RMQ) for its connection to discrete dynamics systems theory and return mapping techniques. The algorithm begins by taking spike times and a concurrent oscillation to which the spikes' phase relationship is in question. Since the phase of the oscillation needs first to be determined, a signal should be of sufficiently narrow bandwidth to admit a reasonable approximation of phase by way of the Hilbert transform. The Hilbert transform is taken to be the imaginary component of the analytic signal, with the untransformed signal as the real component. Each point of the analytic signal is passed as the argument to the arctan2 function to derive an approximation of the untransformed signal's phase over time. This phase time series is cyclic modulo 2π radians. Spike times are next transformed into spike phase with respect to the input oscillation by projecting them onto the oscillation phase time series. Next, the spike phase central tendency is taken on each period of the oscillation to generate a sequence of average phases over the time series. The measure of central tendency selected for experimentation was the geometric mean, since taking the median instead does not return appreciably different results (preliminarily speaking) and more complicated methods such as a kernel density estimation rely on either costly optimizations or potentially dubious assumptions. Furthermore, in the case of a non-bursting input, this step simplifies merely to transforming spike times to spike phases (assuming that there is never more than one spike per cycle) so this algorithm should generalize well to less complicated dynamics.

Suppose that the spike phase central tendency sequence is of length $n \in \mathbb{N}$ and given by $\{\phi_i\}_{1 \leq i \leq n}$ for $0 \leq \phi_i < 2\pi$. Suppose also that $i, j \in \mathbb{N}$ and $k = j - 1$. Then the next step is to form a sequence of $n - 1$

differences given by:

$$\{\eta_k\}_{1\leq k\leq n-1} = \{\phi_{j-1} - \phi_j\}_{2\leq j\leq n} \tag{8}$$

Finally, the output metric of the algorithm which will be denoted by ϑ and is given by the central tendency of the above sequence. The geometric mean is a suitable choice for the same reasons as were considered for spike phase central tendency computation on individual cycles of the input oscillation. Furthermore, we have that $-2\pi < \vartheta < 2\pi$ and in the case of the geometric mean:

$$\vartheta = \frac{1}{n-1}\sum_{k=1}^{n-1}\eta_k. \tag{9}$$

For the RMQ to be an experimentally useful quantification, it is required to reflect model ground truth over a broad range of dual oscillator inputs and simultaneously over variation of key biologically-relevant model control parameters. In (1), it was shown that the superposition of two sine waves of equal amplitude and differing frequency has a readily interpretable beat and carrier frequency. However, when the two amplitudes are not equal it is generally nontrivial to analytically compute beat and carrier frequencies. To illustrate, we manipulate equation (1) but for two amplitudes A_1, A_2 with $A_1 \neq A_2$. Henceforth, for the purposes of modeling, let $A_1 sin(\omega_1 t)$ represent a parameterized theta oscillation and $A_2 sin(\omega_2 t)$ be a parameterized interference oscillation. Then ω_1, ω_2 are the angular frequencies of the theta and interference oscillator respectively and t remains time. Using the identity (1), it is simple to show that superposition of theta and interference oscillations of different amplitudes is disanalogous to (1).

$$\begin{aligned} A_1 sin(\omega_1 t) + A_2 sin(\omega_2 t) &= A_1 sin(\omega_1 t) + A_1 sin(\omega_2 t) + (A_2 - A_1) sin(\omega_2 t) \\ &= 2A_1 cos\left(\frac{\omega_1 - \omega_2}{2} t\right) sin\left(\frac{\omega_1 + \omega_2}{2} t\right) + (A_2 - A_1) sin(\omega_2 t) \end{aligned} \tag{10}$$

Where now the second term $(A_2 - A_1) sin(\omega_2 t)$ in (10) prohibits simply interpretting the cosine and sine arguments in the first term as beat and carrier frequencies respectively. Furthermore, the author is unaware of any method for analytically deriving a closed form solution for the carrier or beat waveforms; in fact, (10) need not even be a periodic function depending on the ratio of ω_1 to ω_2.

When either oscillator amplitude dominates, we expect the burst frequency of the model to approach the frequency of the dominating oscillator. In the case of $A_1 >> A_2$ the model is locked with the phase of the theta oscillator, and when $A_2 >> A_1$ it will exhibit ground truth dynamics as per (2-4). This argument motivates exploration of the region where neither oscillator amplitude dominates and hence model behavior is less predictable. Over the course of all experiments, theta frequency is fixed at 10 Hz with ground truth determined by the choice of interference oscillator frequency, either 9 Hz (recession), 10 Hz (locking) or 11 Hz (precession). A typical simulation set consists of 1600 simulations, each consisting of 100 seconds of synthetic data for each point on a 40x40 mesh defined by the Cartesian product:

$$\{A_{1,i}\}_{1\leq i\leq 40} \times \{A_{2,j}\}_{1\leq j\leq 40} \tag{11}$$

where $\{A_{1,i}\}_{1\leq i\leq 40}$ and $\{A_{2.j}\}_{1\leq j\leq 40}$ each consist of equidistant points on and including the endpoints of the interval $[20, 50]$. This particular interval was chosen to avoid excessive model hyperpolarization while preventing either oscillator from dominating the input and trivializing the dynamics. RMQ was

computed over the entire mesh and using all 100 seconds of synthetic data. This process results in a 40x40 grid of RMQ values, hence mapping ϑ as a function of theta and interference amplitude. Such a grid will be referred to as an amplitude mesh for the sake of concision. Once a mesh had been simulated for each ground truth, we proceded to repeat the entire experiment on the two Cartesian meshes defined by

$$\{W_{r_i}\}_{1\leq i\leq 4} \times \{W_{d_j}\}_{1\leq j\leq 4} \tag{12}$$

$$\{\mu_i\}_{1\leq i\leq 4} \times \{\sigma_j\}_{1\leq j\leq 4} \tag{13}$$

Where each set consists of linearly spaced values on and including the endpoints of interval $[50,300]$ for $\{W_{r_i}\}$, $[8,60]$ for $\{W_{d_j}\}$, $[0.1,0.8]$ for $\{\mu_i\}$ and $[10,200]$ for $\{\sigma_j\}$. The left endpoint of each of these intervals is the base model parameter set value, and the right endpoint of each was the maximum before either the average number of spikes per burst exceeded 4 over a 100 second simulation or the membrane potential fell below -120 mV. Hence the model was assessed within biologically-motivated constraints and for a broad spectrum of dual oscillator inputs.

Results

The base model developed reliably demonstrates ground truth dynamics when forced with a dual oscillator input where both theta and interference sinusoids have equal amplitudes (figure 1). As explained, ground truth depends on relative oscillator frequencies (2-4). These data are representative of the base model and qualitatively demonstrate that it captures key biological characteristics of interest. First, the model membrane potential remains greater than -120 mV. Next, it exhibits bursting dynamics with a perceptible spike frequency adaptation. Finally, bursts contain 1-4 spikes, typical of hippocampal place cells (Harris et al. 2001).

The RMQ was computed over a 40×40 oscillator amplitude mesh for each ground truth: recession, locking and precession (figure 2). For each, both the theta and interference sinusoid amplitudes took on 40 linearly spaced values on and including the endpoints of closed interval $[20,50]$ in mV. Figure 2 depicts these meshes as contour plots where the coloration indicates RMQ return value at each ordered pair of interference and theta amplitude. On the locking regime mesh, the contour plot describes a flat surface with height zero at all points simulated. On the recession mesh, points proximal to the off-diagonal take on negative values with a minimum of -0.308. At the extremes of the main diagonal, RMQ return value is less than 0.01. These results are not erroneous, however there is a band which runs parallel to the off-diagonal but with $A_2 > A_1$ where the RMQ strongly indicates a phase precession regime with maximum value 0.427. By Plotting the time series under these conditions (figure 3.A), it can be seen that initial bursts over a single envelope transiently straddle the boundaries between cycles, generating average cycle spike phases which erroneously indicates rapid precession, despite the clear presence of a gradual recession later in the envelope. Hence, the RMQ returns type I error under some conditions.

Unlike the recession mesh, RMQ values over the precession mesh reflect ground truth or else are approximately zero; taking on a minimum value of -0.065 in the relatively small locking regimes and maximum value of 0.469 over the broad off-diagonal region indicating precession. Upon examination of an individual envelope from the timeseries in what was indicated to be a locking regime (figure 3.B), it can be seen that average cycle spike phase first precesses, then recesses over the terminal 2-3 cycles; over the data examined, this appears to result from transient behavior where two bursts occur at the edges of an individual cycle, erroneously indicating a brief recession. Two bursts on an individual cycle can

only occur when burst frequency exceeds theta, which is definitionally speaking a characteristic of phase precession. Hence, RMQ indication of locking dynamics in these small regions appears to be type II erroneous.

RMQ return values over the dual oscillator amplitude mesh was invariant under variation of adaptation response (W_r) and decay (W_d) for the recession (figure 4), locking (figure 5) and precession (figure 6) regimes. Under all three regimes, the contour plot topology did not noticably differ from that which was in the base model, so the same conclusions are drawn. In addition, RMQ does not appear sensitive to modest variation in spike frequency adaptation dynamics.

Discussion

For the base model, RMQ reflected ground truth over a broad range of dual oscillator amplitudes in the case of precession and recession, and over the entire amplitude mesh in the case of phase locking. RMQ was type I erroneous in the case of recession when interference amplitude was sufficiently higher than theta. Finally, it was type II erroneous within a narrow band of interference amplitudes which were sufficiently greater than the concurrent theta amplitude, where it returned values congruent with phase locking with precession ground truth. Before discussing what this means for the experimental usefulness of RMQ going forward, it is worth pointing out that mesh regions where it failed to reflect ground truth were relatively small, especially over the precession meshes – the ground truth dynamics of hippocampal place cells and the primary intended use case of the algorithm.

Initial results presented here suggest that the most appropriate use of this algorithm would be in conjunction with the average cycle spike phases plotted on the input time series (as presented in figure 1 and figure 3) which is an intermediate of the RMQ process. In all cases where RMQ was erroneous, ground truth dynamics were still qualitatively evident by this visualization. Hence, large volumes of data could be processed by RMQ for a first order quantification of phase dynamics, with a qualitative assessment to consider the possibility of error. Furthermore, by these preliminary results, negative values of large magnitude (with the notion of 'large' left undefined, for now) were never erroneous, so such an experimental outcome could be taken with higher confidence.

All RMQ values used to construct contour plots were computed over 100 seconds of artificial data which, except for the stochastic Ornstein-Uhlenbeck influence, was stationary. This is unlike the biological system where the algorithm will be applied. RMQ does permit the specification of window size and location, such that it is computed over an arbitrary duration of input data. Thus, when nonstationarity of data is a concern, one can consider windowing data to encompass only events of interest or active domains of specific neurons. Moreover, RMQ may be most useful as a comparitive metric to assess changes in neural phase dynamics centered around experimental events or under different experimental conditions.

For a more rigorous interpretation of the results, a statistical analysis of RMQ over the meshes needs to be performed. This step is noticeably absent from the project at this point in time. Furthermore, RMQ amplitude meshes under variation of Ornstein-Uhlenbeck process parameters is forthcoming. With a more rigorous interpretation of results presented here plus the impact of stochastic influences on RMQ, it will be ready for application to hippocampal data available on CRCNS – with the HC-11 (Grosmark et al. 2016) and HC-14 (Girardeau et al. 2017) datasets as attractive candidates. In these, animals were

performing simple linear track navigation at the time of data collection, which included both single-unit activity and local field potential recordings. Results from RMQ analysis of this data will be compared to the conventional technique of linear regression to spike phase over a place field (O'Keefe & Recce 1993) and to RMQ analysis outcome of single unit hippocampal data from animals undergoing REM sleep.REM sleep data will be contributed by David Dupret lab, University of Oxford.

References

Bland BH, Andersen P, Ganes T (1975) Two generators of hippocampal theta activity in rabbits. Brain Res 2:199-218.

Bragin A, Jando G, Nadasdy Z, Hetke J, Wise K, Buzsaki G (1995) Gamma (40-100 Hz) oscillation in the hippocampus of the behaving rat. J Neurosci 1:47-60.

Bullock TH, Buzsaki G, McClune MC (1990) Coherence of compound field potentials reveals discontinuities in the CA1-subiculum of the hippocampus in freely-moving rats. Neuroscience 3:609-619.

Burgess N, O'Keefe J (2011) Models of place and grid cell firing and theta rhythmicity. Curr Opin Neurobiol 21: 734-744.

Buzsaki G (2002) Theta oscillations in the hippocampus. Neuron 33:325-340.

Fox SE, Wolfson S, Ranck JB (1986) Hippocampal theta rhythm and the firing of neurons in walking and urethane anesthetized rats. Exp Brain Res 62:495-508.

Gao TM, Pulsinelli WA, Xu ZC (1999) Changes in membrane properties of CA1 pyramidal neurons after transient forebrain ischemia in vivo. Neuroscience 90: 771-780.

Girardeau G, Inema I, Buzsaki G (2017) Simultaneous large-scale recordings in dorsal hippocampus, basolateral amygdala and neighboring deep nuclei and structures in rats performing a spatial aversive task and sleeping. CRCNS.org http://dx.doi.org/10.6080/K0MS3QXD.

Grosmark AD, Long J, Buzsaki G (2016) Recordings from hippocampal area CA1 pre during and post novel spatial learning. CRCNS.org http://dx.doi.org/10.6080/K0862DC5.

Harris KD, Henze DA, Hirase H, Leinekugel X, Dragoi G, Czurko A, Buzsaki G (2002) Spike train dynamics predicts theta-related phase precession in hippocampal pyramidal cells. Nature 417:738-741.

Harris KD, Hirase H, Leinekugel X, Henze DA, Buzsaki G (2001) Temporal interaction between single spikes and complex spike bursts in hippocampal pyramidal cells. Neuron 32:141-149.

Lengyel M, Szatmary Z, Erdi P (2003) Dynamically detuned oscillations account for the coupled rate and temporal code of place cell firing. Hippocampus 13:700-714.

Levy WB, Steward O (1983) Temporal contiguity requirements for long-term associative potentiation/depression in the hippocampus. Neuroscience 8:791-797.

Mason A (1993) Electrophysiology and burst-firing of rat subicular pyramidal neurons in vitro: a comparison with area CA1. Brain Res 600: 174-178.

Muller RU, Bostock E, Taube JS, Kubie JL (1994) On the directional firing properties of hippocampal place cells. J Neurosci 14: 7235-7251.

O'Keefe (1976) Place units in the hippocampus of freely moving rat. Exp Neurol 51:78-109.

O'Keefe J, Recce ML (1993) Phase relationship between hippocampal place units and the EEG theta rhythm. Hippocampus 3:317-330.

Ranck JB (1973) Studies on single neurons in dorsal hippocampal formation and septum in unrestrained rats: part I. Behavioral correlates and firing repertoires. Exp Neurol 41: 462-531.

Robinson NT, Descamps L, Russell LE, Buchholz MO, Bicknell B, Antonov GK, Lau, JY, Nutbrown R, Schmidt-Heiber C, Hausser M (2020) Targeted activation of hippocampal place cells drives memory-guided spatial behavior. Cell 183: 1586-1599.e10.

Royer S, Zemelman BV, Losonczy A, Kim J, Chance F, Magee JC, Buzsaki G (2012) Control of timing, rate and bursts of hippocampal place cells by dendritic and somatic inhibition. Nat Neurosci 15:769-775.

Schmidt R, Diba K, Leibold C, Schmitz D, Buzsaki G, Kempter R (2009) Single-trial phase precession in the hippocampus. J Neurosci 29:13232-13241.

Scoville WB, Milner B (1957) Loss of recent memory after bilateral hippocampal lesions. J Neurol Neurosurg Psychiatry 20:11-21.

Skaggs WE, McNaughton BL, Wilson MA, Barnes CA (1996) Theta phase precession in hippocampal neuronal populations and the compression of temporal sequences. Hippocampus 6: 149-172.

Uhlenbeck GE, Ornstein LS (1930) On the theory of the Brownian motion. Phys Rev 36:823-841.

Figures and Tables

Table 1. Summary of model parameter values chosen for the base model. The mathematical context for these is made evident in (5-7) with the exception of refractory period and spike amplitude, which are imposed conditionally depending on membrane potential at each time step. Spike amplitude is purely cosmetic and chosen arbitrarily.

Parameter Name	Symbol	Value	Units
Threshold	V_T	-40	mV
Time constant	τ_m	10	ms
Resting membrane potential	V_r	-75	mV
Spike amplitude	V_s	50	mV
Refractory period duration	t_R	2	ms
Adaptation response	W_r	50	mV
Adaptation decay	W_d	8	mV
Adaptation time constant	τ_W	10	ms
Weiner process standard deviation	σ	100	mV
Ornstein-Uhlenbeck process mean	μ	0.3	mV
Ornstein-Uhlenbeck time constant	τ_ξ	50	ms

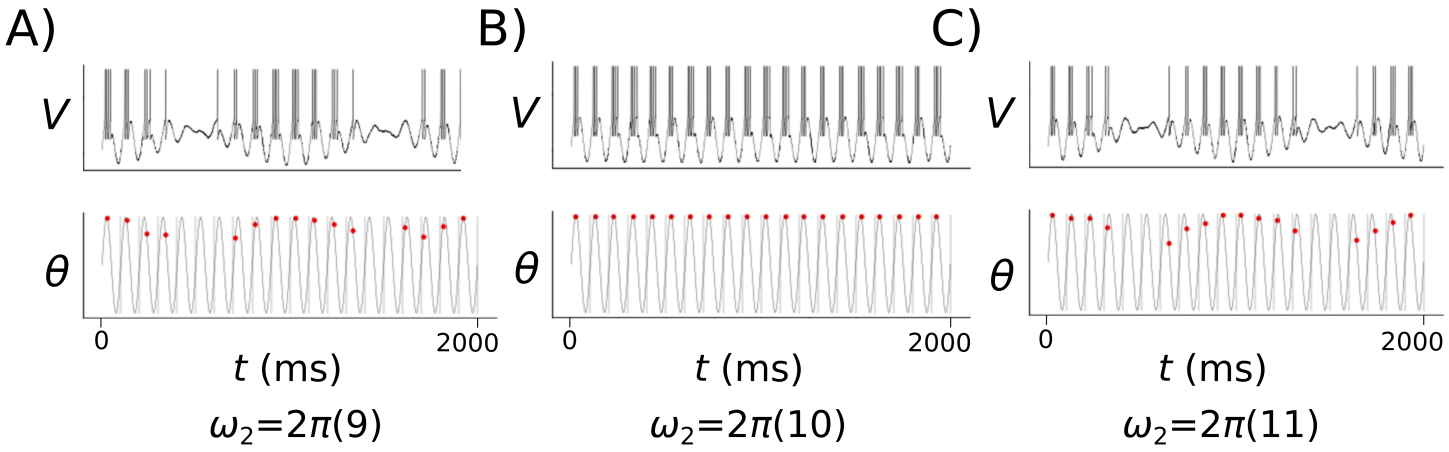

Figure 1. Two second time series generated by base model with varying interference frequency (ω_2) plotted over a sinusoidal model of theta oscillation. Red dots superimposed on theta waveform indicate mean spike phase on each cycle. A) Interference frequency of 9 Hz results in model phase recession as per (2). B) Interference frequency of 10 Hz results in model phase locking as per (3). C) Interference frequency of 11 Hz results in model phase precession as per (4). While left unlabelled to reduce visual clutter, membrane potential remained above -120 mV over the 2 seconds plotted in A, B and C.

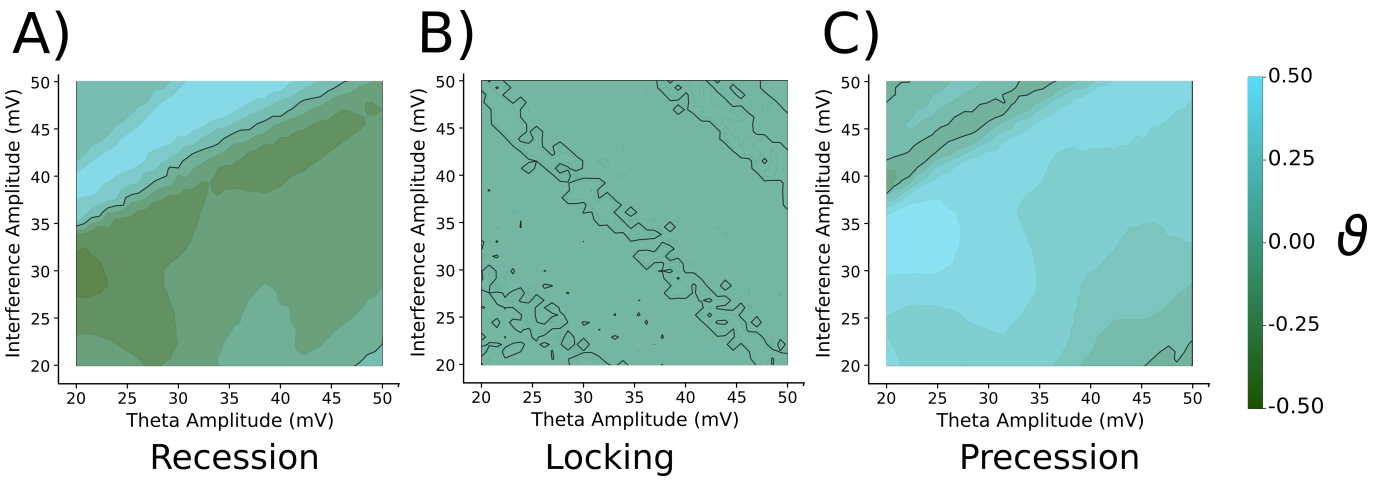

Figure 2. Contour plots depicting RMQ return value (ϑ) as a function of theta and interference oscillator amplitude for the base model under A) recession, B) locking and C) precession regimes. Contour plots are comprised of 1600 values of ϑ arranged in a 40x40 mesh according to the amplitudes of the dual oscillator input used to simulate the data from which it was derived. Magnitude and sign of ϑ is coded by colour according to the colourbar on the right.

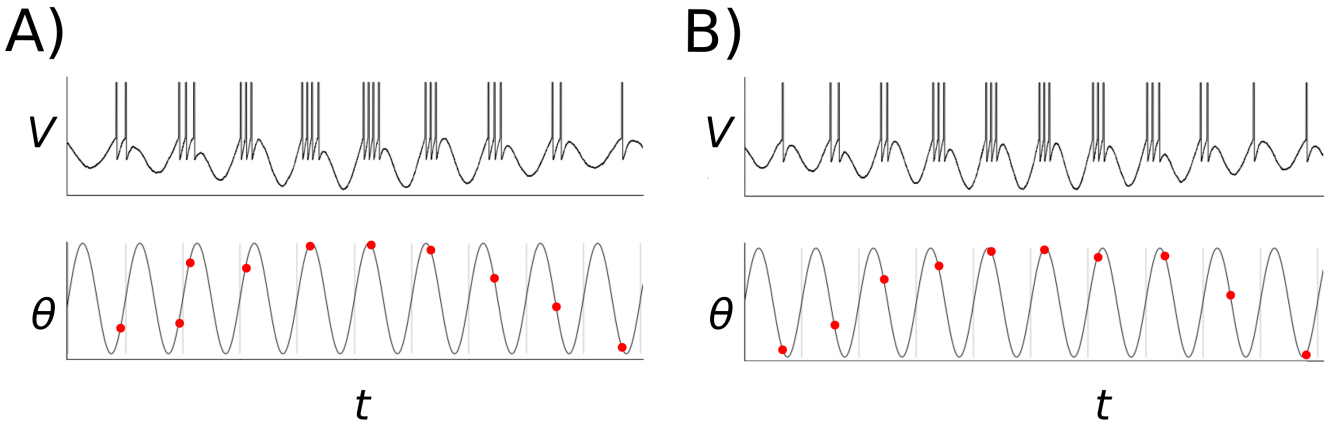

Figure 3. Sample time series generated by base model in regions where RMQ was erroneous. A) Data from precession region in figure 2.A for theta amplitude of 39 mV and interference amplitude of 50 mV. B) Data from locking region in figure 2.C where theta amplitude was 25 and interference amplitude was 43. Red dots superimposed on theta waveform indicate mean spike phase on each cycle.

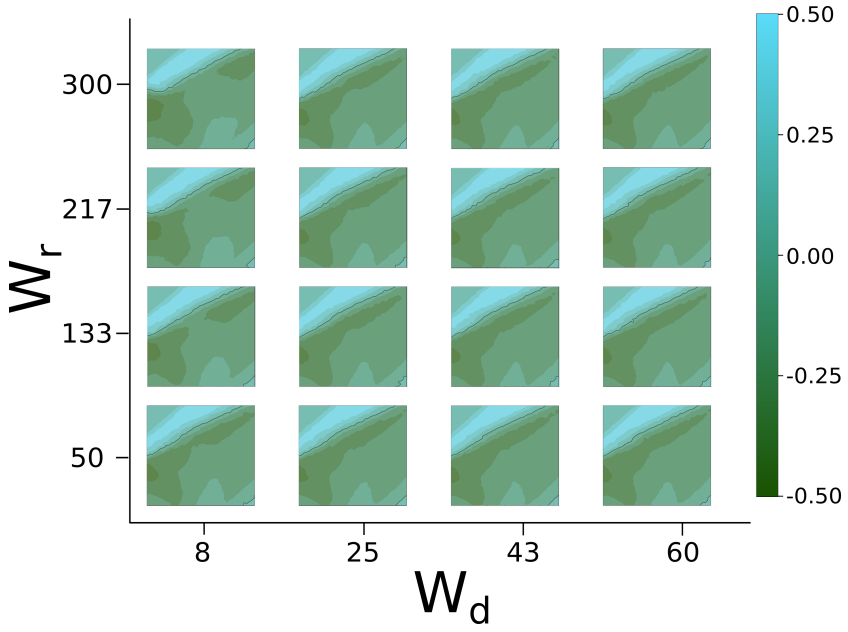

Figure 4. Dual oscillator amplitude mesh contour plots depicting RMQ return value in the case of recession ground truth. Each plot is contructed in precisely the same way as those in figure 2, but with the exception that adaptation response (W_r) and decay (W_d) constants vary over the arranged grid. Magnitude and sign of ϑ is coded by colour according to the colourbar on the right.

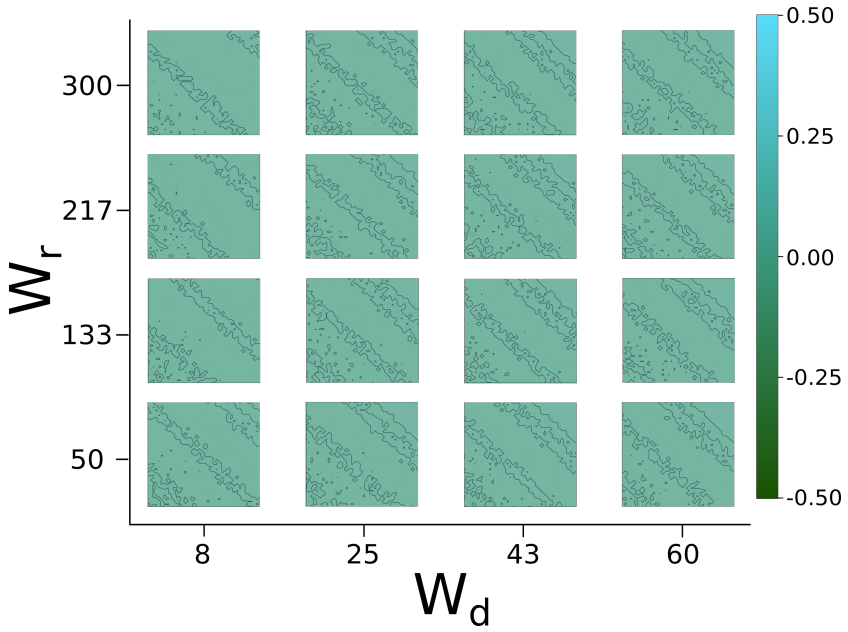

Figure 5. Dual oscillator amplitude mesh contour plots depicting RMQ return value in the case of locking ground truth. Each plot is contructed in precisely the same way as those in figure 2, but with the exception that adaptation response (W_r) and decay (W_d) constants vary over the arranged grid. Magnitude and sign of ϑ is coded by colour according to the colourbar on the right.

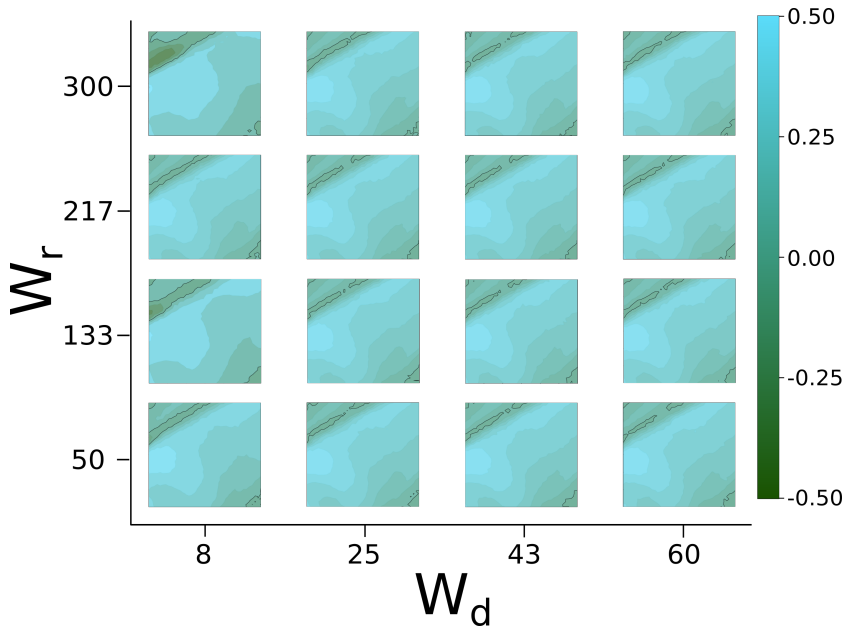

Figure 6. Dual oscillator amplitude mesh contour plots depicting RMQ return value in the case of precession ground truth. Each plot is contructed in precisely the same way as those in figure 2, but with the exception that adaptation response (W_r) and decay (W_d) constants vary over the arranged grid. Magnitude and sign of ϑ is coded by colour according to the colourbar on the right.